$^{15}N^+ + CD_4$ and $O^+ + {}^{13}CO_2$ State-Selected Ion−Molecule Reactions Relevant to the Chemistry of Planetary Ionospheres†

Christian Alcaraz,*,‡ Christophe Nicolas,§,|| Roland Thissen,§ Jan Zabka,⊥ and Odile Dutuit§

LURE, UMR 130, Bât. 209D, Centre Universitaire Paris-Sud, 91898 Orsay Cedex, Laboratoire de Chimie Physique, UMR 8000, Bât. 350, Centre Universitaire Paris-Sud, 91405 Orsay, France, and J. Heyrovsky Institute of Physical Chemistry, Dolejskova 3, CZ 18223 Praha 8 - Kobylisy, Czech Republic

Received: May 23, 2004; In Final Form: September 7, 2004

The dissociative photoionization of N_2 and O_2 by synchrotron radiation in coincidence with threshold photoelectrons is used to produce state-selected N^+ and O^+ atomic ions to study their reactivity. A pure selection of their ground state, $N^+(^3P)$ and $O^+(^4S)$, or excited states, $N^+(^1D)$, $O^+(^2D)$, and $O^+(^2P)$, is obtained by the choice of the photon energy and by further discrimination of atomic ions produced with translational recoil energy. Both reactions studied, $^{15}N^+ + CD_4$ and $O^+ + {}^{13}CO_2$, are of major importance for the chemistry of Titan, Mars, and Venus' ionospheres and are strongly affected by excitation of the parent atomic ion. For the reaction of N^+ with methane, DCN^+ and $DCND^+$ products coming from the decomposition of a long-lived complex are surprisingly not much sensitive to the N^+ excitation, whereas the branching ratio between the dissociative charge-transfer channel, leading to CD_3^+, which is the main product for the ground-state reaction, and the nondissociative charge-transfer channel, leading to CD_4^+, is completely inverted in favor of the latter when N^+ is excited into the ^1D state. This unanticipated result can be well understood by the spin−orbit selection rule in the N^+ recombination. For the reaction of O^+ with carbon dioxide, the reactive channel producing O_2^+, which dominates for the ground-state reaction for thermal collision energies, is completely displaced in favor of the endothermic charge-transfer channel leading to CO_2^+ if either collision energy or O^+ internal energy is brought to the system. The $O^+(^2P)$ metastable state has a larger reaction cross section than the lower ^2D metastable state. Owing to the long lifetime of the N^+ and O^+ metastable states studied here and to their very specific reactivity, they should be individually considered in the models describing the planetary ionospheric chemistry.

Introduction

Reaction dynamics of molecular ions are driven by many forms of energy, in particular, the internal energy of the parent ion. The development of methods, such as the photoelectron photoion coincidence (PEPICO) techniques, to prepare a molecular ion in well-defined states has contributed to a much better fundamental understanding of the unimolecular fragmentation and spectroscopy of these ions and of their bimolecular reactions.[1−8]

Much less is known on the bimolecular reactivity of the excited atomic ions N^+ or O^+ because if one wants to use conventional PEPICO techniques to state select these ions, then one needs in principle to use a source of neutral N or O radicals. Our first fundamental motivation here is to study the effect of the atomic ion electronic excitation on the reaction dynamics. Going from $N^+(^3P)$ and $O^+(^4S)$ ground states to $N^+(^1D, {}^1S)$ and $O^+(^2D, {}^2P)$ excited states brings a few electronvolts to the system and also changes the nature of the initial state. Because these first excited states are known to be very long-lived metastable states,[9] they can be prepared in a low pressure source and their reactivity easily probed later in another part of the experiment. To achieve pure N^+ and O^+ metastable state selection, we have to use more sophisticated selection techniques. Dissociative charge transfer of rare gas cations with O_2 has been successfully used to study many state-selected $O^+(^4S, {}^2D, {}^2P)$ reactions.[7] A second method, derived from the threshold photoelectron photoion coincidence technique (TPEPICO) and based on the dissociative photoionization of O_2, has already been used for the study of the $O^+(^4S, {}^2D, {}^2P) + N_2$ reaction.[10] This second method has been chosen in this work to prepare state-selected $N^+(^3P, {}^1D)$ and $O^+(^4S, {}^2D, {}^2P)$ atomic ions from the N_2 and O_2 precursors.

The second motivation of this study is linked to the chemistry of planetary ionospheres. Very recent or up-and-coming explorations of our solar system planets Mars, Jupiter, and Saturn and their moons, such as Titan (largest moon of Saturn), by spacecrafts, for instance, Mars Global Surveyor, Mars Express, Galileo, and Cassini−Huygens, have motivated extensive efforts to model atmospheres correctly. This also includes laboratory studies to provide accurate inputs or parameters to the models, such as the production and loss rates of the neutral and ionic atmospheric constituents; in particular, for the ionospheric part of the atmosphere, valid photoionization cross sections by solar radiation or electron impact ionization cross sections, ion−molecule reaction or recombination rate constants are needed to model the major ionic species.[11−15] A lot of measurements have already been made and used in modeling planetary atmospheres.[16−20] Usually, models include only ion−molecule

† Part of the special issue "Tomas Baer Festschrift".

* Corresponding author. E-mail: christian.alcaraz@lure.u-psud.fr.
‡ LURE, Centre Universitaire Paris-Sud.
§ Laboratoire de Chimie Physique, Centre Universitaire Paris-Sud.
|| Present adress: Chemical Sciences Division, LBNL Lab., MS 6-2100 1 Cyclotron Road, Berkeley, CA 94720-8226.
⊥ J. Heyrovsky Institute of Physical Chemistry.

10.1021/jp0477755 CCC: $27.50
Published on Web 10/13/2004

reaction rate constants corresponding to the parent ions in their ground state. This is due to the much less amount or even absence of data on the reactivity of excited ions and the enhanced complexity that these metastable species bring to models. However, in planetary ionospheres, these ions are effectively produced by photoionization or by electron impact in long-lived metastable states that do not relax in the ionospheric environment. Such excited species were successfully included in recent models,[11] and their particular activity could be demonstrated. Therefore, it is important to measure the specific reactivity of excited ions to know whether they have to be considered in ionospheric models. It is a long-term activity that we already engaged for molecular ions as shown in our previous studies.[21−24]

Because N^+ and O^+ atomic ions can be directly produced by dissociative ionization of the main neutral constituents, N_2 and CO_2, of Titan and Mars and Venus' atmospheres, respectively (because N_2 refers to Titan and CO_2 to Mars and Venus), they are among the most important ionic species of their respective ionospheres.[11−15] They can be produced in such environment in excited metastable states. Their first excited states, $N^+(^1D)$, $O^+(^2D_J)$ and $O^+(^2P_J)$, have such long lifetimes[9] (269 s for ^1D, 1.6 and 9.1 h for $^2D_{3/2}$ and $^2D_{5/2}$, and 6.3 and 4.9 s for $^2P_{1/2}$ and $^2P_{3/2}$, respectively) that they are not radiatively relaxed during the time between their production and their reaction. Moreover, as they lie 1.9, 3.3, and 5.0 eV above their respective ground states, $N^+(^3P)$ and $O^+(^4S)$, it is expected that, with such an additional amount of energy, the reactivity of these excited species could be very different from that of the ground-state ion and should be characterized.

In the reaction of ground-state N^+ ions with methane, four main ionic products have been identified as CH_3^+, CH_4^+, HNC^+ (or HCN^+), and $HCNH^+$ (or H_2CN^+). The most exothermic channels leading to these products are

$$N^+(^3P) + CH_4 \rightarrow CH_3^+ + NH \qquad \Delta H = -3.4 \text{ eV} \quad \text{(N1)}$$

$$\rightarrow CH_4^+ + N \qquad \Delta H = -1.9 \text{ eV} \quad \text{(N2)}$$

$$\rightarrow HNC^+ + H_2 + H \qquad \Delta H = -2.4 \text{ eV} \quad \text{(N3)}$$

$$\rightarrow HCNH^+ + H_2 \qquad \Delta H = -8.8 \text{ eV} \quad \text{(N4)}$$

We note that other exothermic channels could also lead to the same ions, in particular CH_3^+ ions, which could also be produced by the dissociative charge transfer

$$N^+(^3P) + CH_4 \rightarrow CH_3^+ + H + N \qquad \Delta H = -0.2 \text{ eV} \quad \text{(N1′)}$$

The branching ratio between these products measured in an ion cyclotron resonance (ICR) study,[18] 0.53:0.05:0.10:0.32 for $CH_3^+/CH_4^+/HNC^+/HCNH^+$, is in good agreement with other published values.[25−28] Note that in a very recent experiment,[19] to be more representative of the ions present in Titan's atmosphere, higher pressures of the methane target gas were used to allow the primary product ions to undergo further chemistry. The numeric modeling of the data which includes consecutive reactions leads to a 0.38:0.03:0.15:0.44 branching ratio for the primary $N^+ + CH_4$ reaction quite different from that of previously reported studies made at lower pressures.[18,25−28] The total rate constant measured at 300 K[18,19,25−28] is found to be between 9.4×10^{-10} cm^3 s^{-1} and 14×10^{-10} cm^3 s^{-1}. The rate constant value, 8.2×10^{-10} cm^3 s^{-1}, measured at very low temperature, 8 K, with the CRESU (Cinétique de Réactions en Ecoulement Supersonique Uniforme) technique,[29] is close to the 300 K values. In many reactions of N^+ with hydrocarbons, including methane, Kusunoki and Ottinger et al.[30,31] have identified the $NH(A^3\Pi)$ chemiluminescence in a large range of collision energies. It means that, for the reaction with CH_4, the CH_3^+ product comes at least partly from the N1 channel.

To our knowledge, no reaction of pure metastable N^+ state has been reported in the literature. In several N^+ reaction studies, dissociative ionization of N_2 by electron impact is used to produce excited N^+, but only a fraction of the N^+ population is in a metastable state. In the first ones,[32,33] a 15% population of the first metastable state ^1D is estimated, with the remaining population in the ground state ^3P. In another one,[27] an unknown mixture of $^1D/^1S/^5S$ metastable states is believed to constitute 30% of the population, with the remaining 70% in the ground state ^3P. This last work[27] is, to our knowledge, a unique study of the reaction of metastable N^+ ions with methane. For the reaction of N^+ metastable ions, they report a total rate constant equal to the rate constant of ground-state ions, 1.1×10^{-9} cm^3 s^{-1}, and the inferred branching ratio found between the four main products $CH_3^+/CH_4^+/HNC^+/HCNH^+$ is 0.2:0.1:0.3:0.4.[27]

Remarkably, extensive efforts have been done to characterize the effects of all of the forms of energy on the $O^+ + CO_2$ reaction, including the O^+ electronic energy,[34−36] the vibrational and rotational energy of CO_2[37] related to the temperature, and the mean collision energy, which can be controlled either by the temperature[35,37−46] or by the translational energy of O^+ ions.[34,36,37,47−53] The transition state theory has been also used to model these effects.[54]

For the ground-state $O^+(^4S)$ reaction, only one exothermic channel is open at thermal collision energy, which leads to O_2^+ formed by the decomposition of a long-lived complex

$$O^+(^4S) + CO_2 \rightarrow O_2^+ + CO \qquad \Delta H = -1.2 \text{ eV} \quad \text{(O1)}$$

The isotope distribution of the $^{32}O_2^+$, $^{34}O_2^+$, and $^{36}O_2^+$ products observed in the ion−molecule reactions occurring in an equimolar $C(^{16}O)_2 + C(^{18}O)_2$ mixture suggests that the form of the complex is $(OO\cdots CO)^+$ rather than a CO_3^+ form where all oxygens are equivalent.[48]

When collision energy is increased, a new product, CO_2^+, is formed, as suggested first by Schildcrout,[49] through the slightly endothermic charge transfer, which becomes rapidly the dominant channel

$$O^+(^4S) + CO_2 \rightarrow CO_2^+ + O \qquad \Delta H = +0.16 \text{ eV} \quad \text{(O2)}$$

At even higher collision energy, above 6 eV in the center of mass frame, minor products, CO^+ and C^+, are also observed and attributed to sequential dissociative charge transfers[7,53]

$$O^+(^4S) + CO_2 \rightarrow CO^+ + O + O \qquad \Delta H = +5.9 \text{ eV} \quad \text{(O3)}$$

$$\rightarrow C^+ + O + O + O \qquad \Delta H = +14.3 \text{ eV} \quad \text{(O4)}$$

rather than to the less endothermic channel

$$O^+(^4S) + CO_2 \rightarrow CO^+ + O_2 \qquad \Delta H = +0.7 \text{ eV} \quad \text{(O5)}$$

In the 150−900 K temperature range[35,37−46] or for collision energies below few eV,[37,47−53] the overall rate constant is almost

constant or slightly decreasing with temperature or collision energy and its value lies between 12×10^{-10} and 6×10^{-10} $cm^3\ s^{-1}$. The fraction of CO_2^+ products, however, strongly varies with energy. Viggiano et al. have noted that all types of energy seem to be equally efficient in promoting the endothermic charge-transfer channel and that it is the total amount of energy that is the important parameter.[37]

The O_2^+ and CO_2^+ cross sections or rate constants for the metastable states have been derived from experiments where mixture of states were present. Electrons of variable energy in impact sources were used to produce the $O^+(^4S)$ ground state or a mixture of ground state and metastable states for kiloelectronvolt collisions.[34] They estimated from monitor reactions that the fraction of metastable species (30%) is composed of only the $O^+(^2D)$ state,[34] but this is reconsidered in another kiloelectronvolt collision study.[36] Monitor reactions can also be used as a filter to eliminate the metastable states from $O^+(^4S, ^2D, ^2P)$ mixtures.[35,36] This method has allowed for the study of the reaction for either the ground state, $O^+(^4S)$, or for a mixture of $O^+(^2D, ^2P)$ metastable states at thermal[37] or kiloelectronvolt[36] energies. For thermal energies, $O^+(^2D, ^2P)$ is found to react with the same total rate constant as $O^+(^4S)$ but to produce almost exclusively (95%) the charge-transfer product CO_2^+.[37] At kiloelectronvolt energies, we note that the charge-transfer cross section seems to be lower for the metastable states than that for the ground state[34,36] at all energies between 0.5 and 5 keV.

To produce pure population of O^+ metastable states, two of the methods already presented above[10] have been used, but none of them to probe the O_2^+ and CO_2^+ productions in the present $O^+ + CO_2$ reaction. The one based on the dissociative charge transfer of rare gas cations on O_2[50] has been used to study the dissociative charge transfer (O3) producing CO^+ at collision energies above 6 eV.[7]

In the following section, after the general description of the experimental setup devoted to the study of ion−molecule reactions, we will show how the dissociative photoionization of N_2 or O_2 can be used together with the TPEPICO coincidence technique to prepare N^+ or O^+ atomic ions in well-controlled internal and translational energy. It is applied here to the study of the $^{15}N^+(^3P, ^1D) + CD_4$ and $O^+(^4S, ^2D, ^2P) + {}^{13}CO_2$ reactions. Our results will then be presented and discussed on two points of view, (i) understanding the influence of internal and collision energy on the reaction mechanism and (ii) finding the importance of metastable ions in ionospheric models.

Experimental Methods

The experimental setup, called CERISES (collision et réaction d'ions sélectionnés par electron de seuil) and the methods used in this work to study state-selected ion−molecule reactions have already been described in detail.[22,55,56] Only the important points will be presented here, focusing special attention on the method used to produce state-selected N^+ and O^+ atomic ions. Briefly, it consists of an ion source and a quadrupole−double octopole−quadrupole device.

A. General Considerations. Usually, when a stable neutral M precursor is available, M^+ molecular ions are produced in the source region by the simple photoionization of M by the monochromatized vacuum ultra violet (VUV) synchrotron radiation. Here, to produce N^+ and O^+ ions, we have chosen to use the dissociative photoionization of N_2 and O_2, respectively. To this purpose, we used the SA63 bending magnet beamline on the 800 MeV Super-ACO storage ring to provide monochromatized photons in the 24−27 eV (N_2) and 18−24 eV (O_2) VUV energy range. The parent atomic ions are extracted from the source and injected in the first quadrupolar mass filter in which they are separated from other ions with different masses, in particular, from nondissociated N_2^+ (O_2^+) ions. They are then conducted by a first radio frequency (RF) octopolar guide to the reaction cell, which constitutes the end of this octopole. All parts of the setup before the cell are held in high vacuum (in the range of 10^{-5} mbar in the source and 10^{-6} mbar in the first octopole) to avoid unwanted relaxation by collision to occur.

The reaction takes place in the cell with thermal (300 K) neutral target molecules, CD_4 or CO_2. The isotopically labeled $^{15}N^+$ and the deuterated methane have been chosen here to avoid any mass overlap that would have occurred in the $^{14}N^+ + CH_4$ reaction; therefore,$^{15}N_2$ (Eurisotop, France) and CD_4 (Cambridge Isotope Laboratories, Switzerland) gases with 99.4 and 99% isotopic enrichment, respectively, were used as the precursor and target gas. For the $O^+ + CO_2$ reaction, no mass overlap was expected, and regular research grade O_2 gas was used. However, $^{13}CO_2$ gas was used because the experiments were done in a short measurement session during the study of ion−molecule reaction of $^{13}CO_2^{2+}$.

The voltage difference between the reaction cell and the parent ion formation zone defines the parent ion translational energy from which the mean collision energy in the center of mass frame is derived. The translational energy distribution of the primary ion beam is related to the thermal motion of the N_2 (O_2) precursor, to the finite dimension of the photoionization region in the source, where a uniform electric field is applied to extract the photoions and to the transfer from axial to perpendicular motion in the first quadrupolar mass filter. Its width is the same in the continuous and pulsed acquisition mode, which will be described below. The translational energy distribution of the primary ion beam is derived from the measurement of the primary ion yield as a function of the reaction cell voltage and contributes to about 0.2 eV of the width of the collision energy distribution (fwhm). Depending on the mean collision energy, the thermal motion of the CD_4 (CO_2) neutral target further enlarges this distribution. In principle, another factor, specific to the atomic ion production that is used here, should be considered. Because N^+ (O^+) ions are formed by dissociative photoionization, the kinetic energy release in N^+ (O^+) fragments could modify the parent ion translational energy distribution. We will see below that it is not the case here.

The ionic products are extracted from the cell and guided along a second 42-cm-long RF octopolar device to measure the product ion time-of-flight (TOF) distributions. TOF spectra are obtained by the extraction of the parent ions from the source either with a 800-Hz pulsed field (pulsed acquisition mode) or in coincidence with threshold electrons (coincidence mode). In the first case, the internal energy of parent ions is not selected. After a calibration procedure, these TOF distributions are inverted into product axial velocity distributions, giving very important information concerning the reaction mechanisms. The ionic products are mass selected in a second quadrupolar mass filter and finally counted on a two-stage multichannel plate detector.

B. N^+ (O^+) State Selection. At a given photon energy, $h\nu$, above the limit of the M_2 (M = N or O) dissociative photoionization, M_2^+ and M^+ ions can be formed following the process

$$M_2 + h\nu \rightarrow (M_2^+)^* + e^- \rightarrow M^+ + M + e^- \qquad (1)$$

and the initial energy $h\nu$ is distributed according to

$$h\nu - IP(M_2) = E_i(M_2^+) + E_k(e^-) = D_0(M^+ - M) + E_i(M^+) + E_i(M) + E_k(M^+) + E_k(M) + E_k(e^-) \quad (2)$$

where $IP(M_2)$ is the M_2 ionization potential, $D_0(M^+ - M)$ is the M_2^+ dissociation energy, and E_i and E_k are the internal and kinetic energies, respectively. Moreover, if $h\nu$ is sufficiently high, not only the first dissociation limit associated with ground-state M^+ ions and M atoms can be reached but also higher dissociation limits, associated with either excited M^{+}* ions or excited M* atoms.

For the case of N_2 and O_2 dissociative ionization, the dissociation limits important for this work are given in Table 1 together with their energies.

TABLE 1: N_2 and O_2 Dissociative Ionization Limits and Their Energies Relative to the Ground State of the Neutral Molecule N_2 or O_2

no.	dissociation limit for N_2	E (eV)	dissociation limit for O_2	E (eV)
1	$N^+(^3P)+N(^4S)$	24.29	$O^+(^4S)+O(^3P)$	18.73
2	$N^+(^1D)+N(^4S)$	26.19	$O^+(^4S)+O(^1D)$	20.70
3	$N^+(^3P)+N(^2D)$	26.68	$O^+(^2D)+O(^3P)$	22.06
4	$N^+(^1S)+N(^4S)$	28.35	$O^+(^4S)+O(^1S)$	22.92
5			$O^+(^2P)+O(^3P)$	23.75
6			$O^+(^2D)+O(^1D)$	24.03

For energies above the first dissociation limit, if no selection of the photoelectron energy is performed, both ions M_2^+ and M^+ are produced. However, in a TPEPICO experiment, that is, if only the (M_2^+)* ions produced in coincidence with very low kinetic energy photoelectrons are extracted, then all of the available energy, $h\nu - IP(M_2)$, is converted into internal energy of (M_2^+)* ion, which fragments. However, nothing prevents several energetically accessible dissociation limits to be simultaneously populated; for instance, that is the case for the N_2 dissociative photoionization that we have studied in a previous TPEPICO experiment.[57] Hence, we showed that, in the photon energy range of 26.2−26.7 eV between the limits of the second and third dissociation limits, $N^+(^1D) + N(^4S)$ and $N^+(^3P) + N(^2D)$, about 60% of the N_2^+* ions fragment toward the second dissociation limit, thereby producing $N^+(^1D)$ metastable ions, and 40% toward the first limit, $N^+(^3P) + N(^4S)$, leading to ground-state $N^+(^3P)$ ions. This shows that, with the TPEPICO technique alone, the dissociative photoionization of M_2 does not allow us to produce pure state-selected M^+ fragment ions. To select only one dissociation limit, and hence only one M^+ state, a further discrimination of M^+ fragments according to their recoil kinetic energy is necessary as shown by eq 2.

In the previous study,[57] which was done in a different experimental setup, all N^+ fragments were collected regardless of their recoil energy. Here, in the CERISES setup, a strong geometrical discrimination of fragment ions with recoil kinetic energy is made by using a weak extraction field (1.2 V/cm) and a small 2-mm-diameter hole at the source exit.

The result of such discrimination for the N_2 (O_2) dissociative ionization is shown in Figure 1 where the number of N^+ (O^+) ions extracted from the source in coincidence with threshold photoelectrons is plotted as a function of photon energy. In the Figure, false coincidences, measured at each photon energy, have been subtracted.

For the N_2 case (Figure 1a), a first peak is observed at about 24.3 eV, which is the onset of the N_2^+ dissociation leading to the first limit, $N^+(^3P) + N(^4S)$. At this energy, N^+ and N fragments can only be produced without recoil kinetic energy.

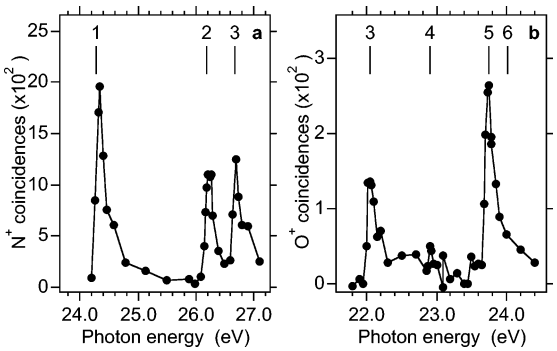

Figure 1. TPEPICO spectra of N^+ (a) and O^+ (b) in the dissociative photoionization of N_2 and O_2, respectively, recorded as a function of photon energy with strong kinetic energy discrimination of the atomic fragment ions. The small vertical lines labeled 1−3 in a and 3−6 in b indicate the energy positions of the dissociation limits given in Table 1.

When the photon energy is increased above 24.3 eV, N^+ ions are produced with increasing recoil energy and are thus strongly discriminated. At 26.2 eV, the onset for the second limit, $N^+(^1D) + N(^4S)$, a second peak is observed because, at this energy, N^+ ions are again produced without any recoil energy. If the decrease in the N^+ yield measured below 26 eV is extrapolated to 26.2 eV, the photon energy of the second peak, it reaches the noise level. Hence, at 26.2 eV, almost pure production of $N^+(^1D)$ metastable state is achieved. The number of measured N^+ counts is used to evaluate the statistical noise level and leads to an estimate of the error in the internal state population lower than 3% limited by the acquisition time. Hence, the $N^+(^1D)$ population is greater than 97%. At 26.7 eV, we observe a third peak corresponding to the third dissociation limit, $N^+(^3P) + N(^2D)$. This peak is also associated with the production of ground-state $N^+(^3P)$, but to produce it, it is safer to set the photon energy at 24.3 eV (first peak) to avoid any possible contamination from the $N^+(^1D)$ metastable state.

The same behavior is observed for the O_2 case (Figure 1b). The two peaks labeled 3 and 5 correspond to the third and fifth dissociation limits, $O^+(^2D)+O(^3P)$ and $O^+(^2P)+O(^3P)$, respectively (Table 1). These two limits are known to be very efficiently populated at their threshold in coincidence with threshold electrons by dissociative photoionization of O_2 in the region of the $III^2\Pi u$ state of O_2^+.[58−61] Between the two peaks, a much less intense structure is also visible and corresponds to the fourth dissociation limit, $O^+(^4S)+O(^1S)$. Again, if we consider the signal levels at the maximum of peaks 3 and 5 and just below each of them, one clearly sees that nearly pure population of $O^+(^2D)$ and $O^+(^2P)$ metastable states can be produced if we set the photon energy at 22.06 and 23.75 eV, respectively. If the number of measured O^+ counts is also used to evaluate the statistical noise level, then one can say that the purity of $O^+(^2D)$ and $O^+(^2P)$ metastable states produced on these two peaks is higher than 92 and 94%, respectively. The production of O^+ in its ^4S ground state is achieved by setting the photon energy to 18.73 eV, the first dissociation limit.

A comparison of this technique should be made with the other methods that have been used to produce N^+ or O^+ metastable states. The first advantage over methods such as the one using electron impact with variable electron energy is that pure populations of either the ground state or excited states are produced. Moreover, as just shown, the variation of the TPEPICO M^+ yield as a function of photon energy is a direct measure of the purity of the excited-state population; thus, we do not need a monitor reaction or the reaction to be studied

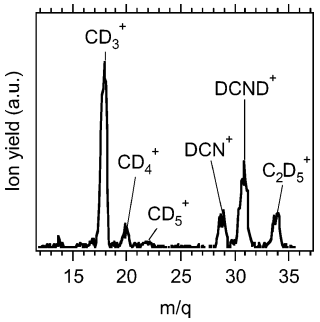

Figure 2. Product ion mass spectrum for the $^{15}N^+ + CD_4$ reaction at a collision energy of $E_{CM} = 0.3$ eV recorded at a photon energy of 25.1 eV.

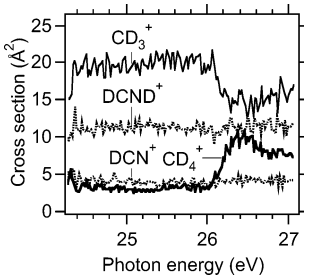

Figure 3. Absolute cross sections of the $^{15}N^+ + CD_4$ reaction for the CD_3^+, CD_4^+, DCN^+, and $DCND^+$ products at a collision energy of $E_{CM} = 0.3$ eV. All $^{15}N^+$ parent ions produced by dissociative photoionization which exit the source are allowed to react. As a function photon energy, they correspond to ^3P ground state or a mixing of ^3P and ^1D state above 26.2 eV.

itself to extract an estimate of the population ratio between the various states.

Another point of comparison comes from the fact that, as it was described above, we need to discriminate between two populations of hot ground-state ions and cold excited ions to achieve the state selection. This is also the case when dissociative charge transfer of rare gases R^+ (R = He, Ne, and Ar) on O_2 in a radio frequency (RF) ion guide is used to produce state-selected $O^+(^4S,^2D,^2P)$ ions.[62] In this case, they also take advantage of the different translational energy distributions of O^+ product ions in the ^4S,^2D, and ^2P states. However, in this case, because all of the distributions have finite widths with partial overlap, one has to find an optimum collision energy and an appropriate RF amplitude and frequency to allow the best discrimination between them.[62] This is not an easy task because it strongly depends on a good a priori knowledge of the reaction dynamics. Nevertheless, this was possible in the case of O_2, for which they succeed in producing each of the $O^+(^4S)$, $O^+(^2D)$, and $O^+(^2P)$ states by charge transfer with Ar^+, Ne^+, and He^+, respectively.[62] The purity of the $O^+(^2D)$ state was more than 90% and was estimated to be between 85 and 96% for the $O^+(^2P)$ state.

Our present method has three advantages. First, the state-selected fragment ion has zero kinetic energy, thus it is much easier to separate it from energetic ions. Second, the kinetic energy of all fragments is perfectly known. The third advantage concerns the collision energy distribution, which is an important parameter for the reaction dynamics. Because the state-selected fragment ion has no recoil energy, there is no broadening of the collision energy distribution induced by the fragmentation process, whereas when dissociative charge transfer of rare gases on O_2 is used, the O^+ ion products have some kinetic energy due to the exothermicity of the charge-transfer reaction.[7] To reduce the translational energy distribution to 0.5 eV, they used a differential retarding potential method.[63]

However, not all states are produced by dissociative ionization; for instance, we have not been able to produce any $N^+(^1S)$ state near 28.35 eV, the energy of the fourth dissociation limit $N^+(^1S) + N(^4S)$, in the dissociative photoionization of N_2.[22] Another drawback of the method is the inherent low signal associated with coincidence techniques.

Results

A. $^{15}N^+ + CD_4$ Reaction. *1. Continuous Acquisition Mode.* Figure 2 shows an example of a mass spectrum recorded at mean collision energy of 0.3 eV in the CM frame.

In this experiment, the dissociative photoionization of N_2 has been used to produce the N^+ parent ions. For a better sensitivity, ions are continuously extracted from the source toward the reaction cell. The maximum N^+ ion yield is at 25.1 eV of photon energy. This efficient mode of acquisition, called the continuous mode, is very useful for a first exploration of the system. Because 25.1 eV is below the second limit of dissociation, all N^+ parent ions are in the ^3P ground state.

The ion yield shown in Figure 2 is actually the difference between two spectra recorded with the target gas put in the reaction cell or in the main chamber to get rid of the ions produced outside the cell. It is why the $^{15}N^+$ parent ion signal does not appear at mass (m/q) 15. As observed in previous studies, the four main products of CD_3^+, CD_4^+, DCN^+ (DNC^+), and $DCND^+$ (D_2CN^+) are observed at masses 18, 20, 29, and 31, respectively. The signal at mass 22 and 34 is attributed to CD_5^+ and $C_2D_5^+$ products, which result from the secondary reactions $CD_4^+ + CD_4$ and $CD_3^+ + CD_4$, respectively, as can be demonstrated by varying the pressure of the target gas. Because these reactions are very efficient,[17] the pressure in the cell was kept low to avoid underestimating the CD_3^+ and CD_4^+ productions. Another reaction, $DCN^+ + CD_4$, which is known to efficiently produce $DCND^+$ ions,[17] could have also altered the ratio between DCN^+ and $DCND^+$ products for too large pressures. Very low signals observed at other masses, such as 17 and 19, could be attributed to ND^+ and ND_2^+ minor products. After the subtraction of the $^{13}CD_3^+$ contribution to mass 19, ND_2^+ could only account for less than 0.5% of the products. These minor channels will not be considered in the following.

The continuous mode was also used to have a first qualitative estimate of the effect of N^+ parent excitation. In Figure 3, the absolute cross sections for each of the four main products, measured at a collision energy $E_{CM} = 0.3$ eV, are displayed as a function of the photon energy used to create N^+ ions. The cross sections were derived from the ratio of product to parent ion intensities and from the measurement of the absolute target gas pressure.[21,55,56] The uncertainty on the absolute cross sections is estimated to 25%.

As in the preceding experiment, we know that below 26.2 eV only $N^+(^3P)$ ions can be produced; therefore, in this energy range, the values are actual measurements of the $^{15}N^+(^3P) + CD_4$ reaction cross sections, and as expected, they do not vary with photon energy. Above 26.2 eV, the second dissociation limit is accessible. However, because no selection of the N^+ state is made in the continuous mode, parent ions are formed in a mixture of $N^+(^3P)$ and $N^+(^1D)$ states. In this range, the measurements correspond to an effective cross section for this mixed population. A strong variation is observed at the $N^+(^1D)$ onset for the CD_3^+ and CD_4^+ ion products. Because only a fraction of N^+ ions are in the excited ^1D state, the reaction cross sections for these two products can be predicted to be very

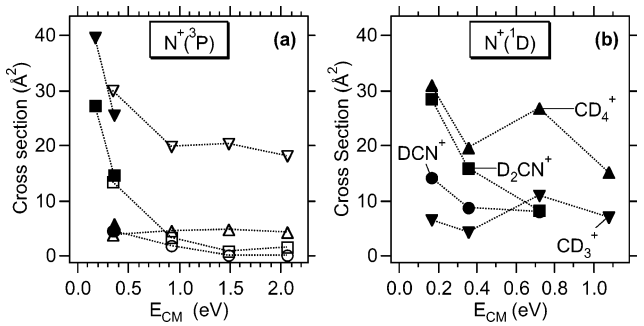

Figure 4. Absolute cross sections for the production of CD_3^+, CD_4^+, DCN^+ (DNC^+), and $DCND^+$ as a function of collision energy for the $^{15}N^+(^3P, ^1D) + CD_4$ reaction. In a, parent ions are prepared in the $N^+(^3P)$ state in coincidence with threshold electrons at 24.3 eV photon energy (full symbols) or in the pulsed mode (see text) at 25.1 eV (open symbols). In b, parent ions are prepared in the $N^+(^1D)$ state in coincidence with threshold electrons at 26.2 eV of photon energy. The symbol correspondence is indicated in b only but is identical in a.

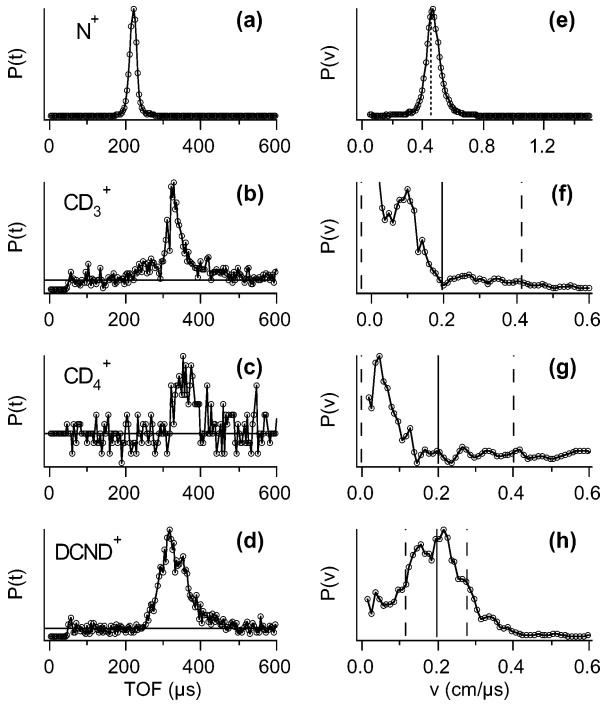

Figure 5. Time-of-flight (left) and axial velocity (right) distributions of $^{15}N^+$ parent ions and CD_3^+, CD_4^+, and $DCND^+$ product ions for the $^{15}N^+ + CD_4$ reaction at a collision energy $E_{CM} = 1$ eV. CD_3^+ and $DCND^+$ products have been recorded for the reaction of $N^+(^3P)$ ground state and CD_4^+ products for the reaction of $N^+(^1D)$ metastable state. Axial velocity distributions are given in the laboratory frame. In e, the vertical dotted line indicates the expected velocity of parent ions. In f−h, the vertical continuous line indicates the velocity of the center of mass, and the dashed lines define the product axial velocity range if the total kinetic energy is the same before and after the reaction.

different for the excited $N^+(^1D)$ state reaction (much lower for CD_3^+ and much higher for CD_4^+). Whereas for the DCN^+ and $DCND^+$ products, the measured effective cross sections do not vary much with photon energy, only a small increase is observed above 26.2 eV for the DCN^+ product. This tells us that N^+ excitation to ^1D is not expected to induce very strong variations on the cross sections for DCN^+ and $DCND^+$ production.

2. Coincidence and Pulsed Acquisition Modes. When ground-state parent ions are extracted in a pulsed mode, either in coincidence with the threshold electron or not, there is a major advantage. Indeed, all product ions are extracted, in particular, those that are backward scattered in the laboratory frame. This is achieved by pulsing the exit electrode of the first quadrupole to reflect backward ions toward the detector. Taking advantage of this, we used two modes to measure the absolute reaction cross section of $N^+(^3P)$ ground state, the coincidence mode and the pulsed mode. The coincidence measurements were made at 24.3 eV of photon energy, which corresponds to the $N^+(^3P)$ onset. The pulsed acquisition mode measurements were made at 25.1 eV of photon energy, which is below the $N^+(^1D)$ onset and corresponds to the maximum N^+ ion yield. The latter mode was used because it gives a better signal-to-noise ratio than the coincidence measurements.

For $N^+(^1D)$ reaction cross section measurements, only the coincidence mode was used at 26.2 eV of photon energy to allow state selection.

Figure 4 shows measured absolute reaction cross sections for both the ^3P and ^1D states of $^{15}N^+$ as a function of collision energy.

For the $N^+(^3P) + CD_4$ reaction (Figure 4a), both modes were used at $E_{CM} = 0.36$ eV and they give very similar results, as expected. The reaction cross section decreases with E_{CM} for all products except for CD_4^+, for which a small cross section almost independent of E_{CM} is measured. DCN^+ and $DCND^+$ cross sections have the same collision energy dependence, which is indicated by data recorded in the continuous mode, not shown here. This decrease with collision energy is a first indication that DCN^+ and $DCND^+$ products come from the decomposition of a long-lived complex. The absence of variation in the CD_4^+ cross section is compatible with a charge-transfer process. At all E_{CM} values, CD_3^+ is by far the main product, and, even if its cross section also clearly decreases with E_{CM}, especially in the lowest range, its dependence is quite different and the cross section reaches a plateau above 1 eV. This more complex behavior of the CD_3^+ cross section will be discussed later. Let us only recall here that it could be formed either from dissociative charge transfer or D^- transfer.

For the $N^+(^1D) + CD_4$ reaction (Figure 4b), a drastic variation in the cross sections with N^+ excitation for CD_3^+ and CD_4^+ products is observed as expected above from the measurements in the continuous mode of the effective cross sections as a function of photon energy. Indeed, a reduction in the CD_3^+ cross section by a factor 7 and an increase in the CD_4^+ cross section by a factor 5 are measured when N^+ is excited into the ^1D state. Whereas for the DCN^+ and $DCND^+$ products, relatively smaller variations of the cross sections are observed. They are higher than the ground-state cross sections by about 90 and 17% for DCN^+ and $DCND^+$, respectively, and they also decrease with collision energy.

Time-of-flight spectra and axial velocity distributions of parent and product ions are shown in Figure 5. Because of the cylindrical symmetry of the experiment, axial velocity distributions $P(v)$ of the reaction products can be derived from the time-of-flight (TOF) distributions $P(t)$ after a calibration procedure of distances and potentials. The most significant examples of the TOF (Figure 5a−d) and axial velocity distributions (Figure 5e−h) in the LAB frame are given for 1 eV of collision energy. The measurements have also been done at $E_{CM} = 0.36$ eV.

As expected for the decomposition of a long-lived complex, the $DCND^+$ velocity distribution (Figure 5h) is symmetric and centered around the center of mass velocity. However, the distribution extends very far on both sides beyond the dashed lines, which correspond to the maximum product axial velocities when the kinetic energy of the reactants and products are the same. Because the channel corresponding to the $DCND^+$ production is very exothermic, it is not surprising that at least

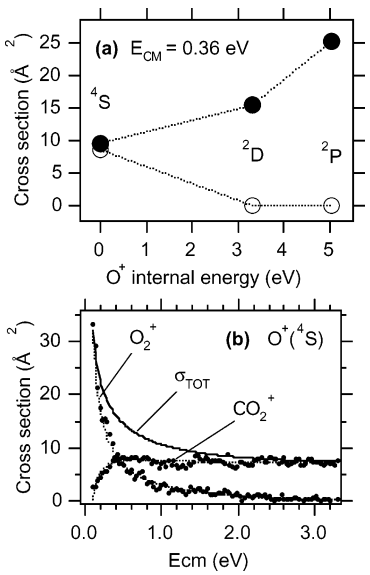

Figure 6. Absolute cross sections of the state-selected $O^+(^4S, ^2D, ^2P) + {}^{13}CO_2$ reaction. (a): In the coincidence mode as a function of O^+ internal energy at $E_{CM} = 0.36$ eV, for O_2^+ (○) and CO_2^+ (●). (b): In the continuous mode as a function of collision energy for the ground-state $O^+(^4S)$. σ_{TOT} is the total cross section summed over O_2^+ and CO_2^+ products (—).

a fraction of the available energy is converted into product kinetic energy. The same behavior is observed for DCN^+ (DNC^+) products.

In contrast, the CD_3^+ and CD_4^+ velocity distributions clearly peak at low velocities in the LAB frame, indicating that these products are emitted backward in the center of mass frame. Quite similar distributions within our resolution are observed for excited ^1D and ground state ^3P reactions for each of these two products. These low velocity distributions are expected in the case of a direct charge transfer (CD_4^+) or dissociative charge transfer (CD_3^+). However, for CD_3^+, the distribution is also compatible with an "D^-" transfer processes for which an osculating complex of short lifetime has been already observed. In such cases, the ND and CD_3^+ product are expected predominantly in the forward and backward hemispheres, respectively.[64]

B. $O^+ + {}^{13}CO_2$ Reaction. We also used two acquisition modes here, the coincidence and continuous modes. The coincidence mode was used at the photon energies 18.73, 22.06, and 23.75 eV to prepare O^+ ions with pure ^4S, ^2D, or ^2P excitation, respectively, but for only one collision energy, $E_{CM} = 0.36$ eV. The continuous mode with photon energies below the first excited dissociation limit was used to look at the $O^+(^4S)$ reaction at other collision energies from 0.1 to 3.3 eV. The reaction cross sections measured for the two observed products, O_2^+ and $^{13}CO_2^+$, are displayed in Figure 6.

For the $O^+(^4S)$ reaction, we see in Figure 6b that, at very low collision energies, only O_2^+ products are formed, as expected, because the charge-transfer channel (O2) is endothermic by 0.2 eV. The small amount of CO_2^+ products at the lowest collision energy is the result of our collision energy resolution. As collision energy is increased, the O_2^+ cross section strongly decreases, which is indicative of a product coming from the decomposition of a long-lived complex. At the same time, the CO_2^+ becomes very rapidly the major product, meaning that the collision energy overcomes the 0.2 eV endothermicity. The total cross section, σ_{TOT}, summed over the two products is displayed in Figure 6b. Its dependence on collision was found to be $(E_{CM})^{-0.47}$, slightly less steep than the capture cross section, whereas the O_2^+ dependence is steeper $(E_{CM})^{-1.1}$.

When the O^+ parent ion is excited to the ^2D or ^2P states, O_2^+ formation is not observed anymore at $E_{CM} = 0.36$ eV, to the precision of our coincidence measurement. This means that CO_2^+ is the unique product (>95%) for the $O^+(^2D) + CO_2$ and $O^+(^2P) + CO_2$ reactions at $E_{CM} = 0.36$ eV. At this collision energy, the $O^+(^2P)$ reaction is about 60% more efficient to produce CO_2^+ than the $O^+(^2D)$ reaction, which was itself already 60% more efficient than the $O^+(^4S)$ reaction to make this product. If we consider the sum over all products, the efficiency ratio of $O^+(^4S)$, $O^+(^2D)$, and $O^+(^2P)$ reactions with CO_2 is 1:0.85:1.40 at $E_{CM} = 0.36$ eV. Because we are giving a relative ratio here, the uncertainties are related to the relative uncertainty of cross section measurements, which, here, is about 10%.

Discussion

A. $^{15}N^+ + CD_4$ Reaction. We have seen that the four main products can be clearly divided in two distinct groups according to the two main classes of processes that account for their production. On one hand, DCN^+ and $DCND^+$ seem to result from the decomposition of a long-lived complex, and on the other hand, the CD_3^+ and CD_4^+ products are associated to more direct processes. However, many important questions remain. First of all, we have to determine the nature of the complex and its decay into many competitive dissociative channels. It is not clear either which of the two channels, the dissociative charge transfer (N1′) or the D^- transfer (N1), is responsible for the CD_3^+ production, and how both processes compete with the non dissociative charge transfer (N2). Finally, one has to describe the competition between the two main classes of processes, and especially here, what the role of parent ion excitation is in these processes. These points will be discussed in the following. But let us first compare our results to what is already known about this system.

1. Total Reaction Cross Section and Branching Ratio. At all collision energies at which the cross sections of the four products were measured, either in the coincidence or in the pulsed mode, the sum of these four values was calculated. It should closely represent the total reaction cross section because these four products are, by far, the major ones. By multiplying the total cross section by the reactant mean relative velocity, it is converted into the total reaction rate constant. These values are reported in Figure 7 as a function of collision energy.

When we evaluate the dependence on collision energy E_{CM} of the total cross section with a functional form $A(E_{CM})^\alpha$, the value found for the α is very close to -0.5. Such a dependence, typical of the Langevin cross section that describes the capture process, is shown by the dotted line in Figure 7a. After conversion, it corresponds to a rate constant of 15×10^{-10} cm^3 s^{-1}, shown in Figure 7b. At 300 K, rate constants reported in the literature[25−28] for the $N^+ + CH_4$ reaction range between 9.4×10^{-10} and 14×10^{-10} cm^3 s^{-1}, and the Langevin cross section itself, which represents the maximum cross section for a capture process, is 14×10^{-10} cm^3 s^{-1}. Our value is slightly higher than these values and is 25% higher than the recommended value,[18] 12×10^{-10} cm^3 s^{-1}. The difference is, however, within the uncertainty of our absolute measurements.

The branching ratio between the four major products CH_3^+/CH_4^+/HCN^+/$HCNH^+$ for the $N^+ + CH_4$ reaction have been reported in the literature.[18,19,25−28] The evaluated values, 0.53:0.05:0.10:0.32, which are used in planetary ionospheric models, were measured at a temperature of 300 K[18] and are shown in Figure 8 together with the branching ratio for the $^{15}N^+ + CD_4$

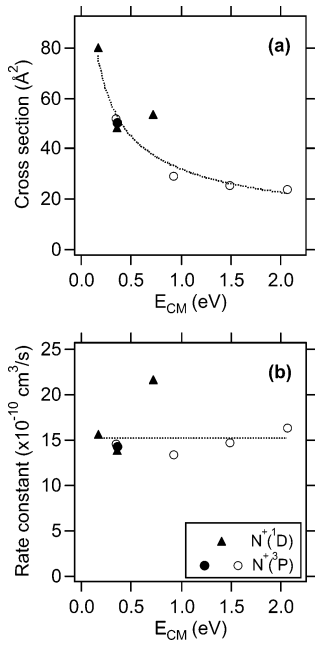

Figure 7. Total cross sections (a) and rate constants (b) summed over CD_3^+, CD_4^+, DCN^+, and $DCND^+$ products for the $^{15}N^+ + CD_4$ reaction as a function of collision energy. $^{15}N^+(^3P, ^1D)$ parent ions are produced in coincidence with threshold electrons (full symbols) or in the pulsed mode (open symbols). The dotted curve in panel a follows an $(E_{CM})^{-1/2}$ dependence and corresponds to a rate constant of 15×10^{-10} cm^3 s^{-1} (dotted horizontal line in b).

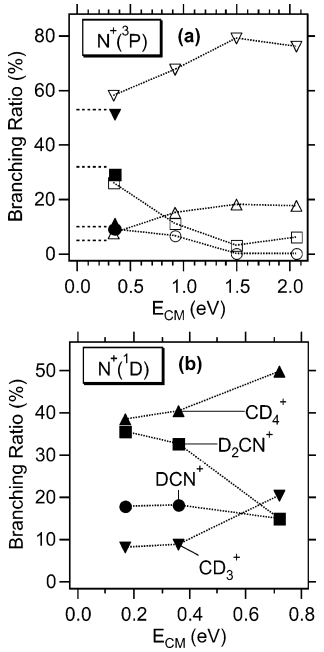

Figure 8. Product branching ratio $CD_3^+/CD_4^+/DCN^+/DCND^+$ for the $^{15}N^+ + CD_4$ reaction with the same notation as that in Figure 4. The corresponding nondeuterated values evaluated in the literature,[18] for the $^{14}N^+(^3P) + CH_4$ reaction at a temperature 300 K, are shown at low energies by a dashed line in a.

reaction measured in this work as a function of collision energy and parent-ion excitation.

For ions in the ground-state $N^+(^3P)$, one sees in Figure 8 that the major effect of collision energy is to favor the products issued from the direct processes, CD_3^+ and CD_4^+, at the expense of the products coming from the long-lived collision complex decomposition, DCN^+ and $DCND^+$, as expected. The values for the coincidence and pulsed experiments at the lowest collision energy, 0.36 eV, are 0.51:0.11:0.09:0.29 and 0.58:0.07:0.09:0.26, respectively, in good agreement with the McEwan[18] values, indicating that there is a negligible isotopic effect.

For excited $N^+(^1D)$ ions, the CD_3^+ and CD_4^+ branching ratios, which also increase with collision energy, are smaller than for the ground-state $N^+(^3P)$ case, and on the contrary, the DCN^+ and $DCND^+$ branching ratios are higher. At $E_{CM} = 0.36$ eV, the branching ratio is 0.09:0.40:0.18:0.33 meaning that the $(CD_3^+ + CD_4^+)/(DCN^+ + DCND^+)$ ratio is equal to 0.62:0.38 and 0.49:0.51 for the $N^+(^3P)$ and $N^+(^1D)$ reaction, respectively. But the major effect of N^+ excitation is a complete reversal of the CD_3^+/CD_4^+ ratio from 4.5:1 to 1:4.7.

Only one work, to our knowledge, reports branching ratios for the reaction of metastable state of $^{14}N^+$ ions with CH_4.[27] The authors estimate that the N^+ population is constituted by 70% of $N^+(^3P)$ ground state and 30% of an unknown mixture of the first three metastable states $N^+(^1D,^1S,^5S)$. For the metastable population only, they infer a product distribution $CH_3^+/CH_4^+/HCN^+/HCNH^+$ equal to 0.2:0.1:0.3:0.4. It is difficult to make a direct comparison of this value to ours, considering the uncertainty of their metastable state composition. However, their ratios $((CH_3^+ + CH_4^+)/(HCN^+ + HCNH^+) = 0.3:0.7$ and $CH_3^+/CH_4^+ = 0.2:0.1)$ suggest that other states than the ^1D state might have been populated in their experiment.

2. Long-Lived Complex. We have shown that the observations made for the $DCN^+(DNC^+)$ and $DCND^+$ $(D_2CN)^+$ products suggest that they result from the decomposition of a long-lived complex. This is not surprising because their production implies the formation of a new C−N bond. Two stable ions $CH_2NH_2^+$ and CH_3NH^+ which lie 11 and 10 eV below the entrance channel $N^+ + CH_4$, respectively, are good candidates to be such a complex.

A fit with the $A(E_{CM})^\alpha$ form of the dependence of DCN^+ and $DCND^+$ cross sections with E_{CM}, gives a value of α equal to −1.5 for the $N^+(^3P)$ reaction, much steeper than that for the Langevin cross section. The difference here is probably the result of the strong competitive processes that lead directly to CD_3^+ and CD_4^+ products before the formation of such a stable complex, which are relatively more efficient at higher collision energies.

We measured that the dissociation of the complex leads essentially to $DCN^+(DNC^+)$ and $DCND^+$ $(D_2CN)^+$ production in a 1:3 ratio. If we consider only the lowest channels that lead to these products, $DNC^+ + D_2 + D$ (−2.4 eV), $DCN^+ + D_2 + D$ (−1.4 eV), $DCND^+ + D_2$ (−8.8 eV), and $D_2CN^+ + D_2$ (−5.5 eV), one sees that the $DCND^+$ $(D_2CN)^+$ production is by far the most exothermic and one could have expected an even lower $DCN^+/DCND^+$ ratio. A complete statistical calculation of the complex dissociation would be highly valuable to make a reliable prediction of this ratio. To this purpose, other channels have to be considered, for instance, the two channels associated with $DCND^+$ $(D_2CN)^+$ triplet states,[65] $DCND^{+*} + D_2$ (−3.3 eV), and $D_2CN^{+*} + D_2$ (−3.2 eV), which are less exothermic. Moreover, sequential dissociations have to be included as well through the three following schemes

$$(NCD_4)^+ \rightarrow (NCD_2)^+ + D_2 \rightarrow (NCD)^+ + D + D_2 \quad \text{(S1)}$$

$$(NCD_4)^+ \rightarrow (NCD_3)^+ + D \rightarrow (NCD)^+ + D_2 + D \quad \text{(S2)}$$

$$\rightarrow (NCD_2)^+ + D + D \quad \text{(S3)}$$

Note that the $(NCD)^+ + D + D + D$ channel, which is endothermic by more than 2 eV, cannot be reached, which explains why scheme S3 ends at $(NCD_2)^+ + D + D$.

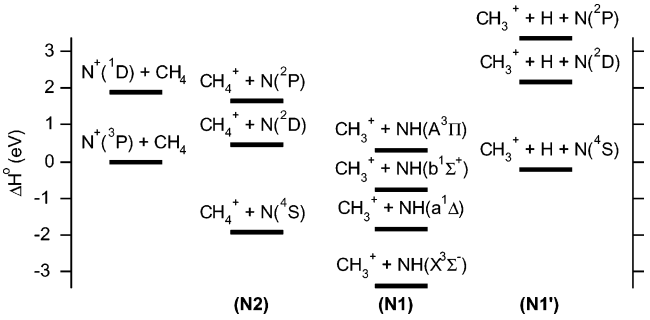

Figure 9. Energy diagram of the $N^+(^3P, ^1D) + CH_4$ reaction for the entrance and N2, N1, and N1′ product channels.

Effect of $N^+(^1D)$ Excitation. Very surprisingly, the DCN^+ and $DCND^+$ products are favored by the parent ion excitation by more than 30%. Because the DCN^+ and $DCND^+$ productions are linked to the complex formation, which is, as already mentioned, in strong competition with the direct processes, the DCN^+ and $DCND^+$ variation could thus result from the effect of the $N^+(^1D)$ excitation on the charge transfer and D^- transfer processes as discussed below.

3. The CD_3^+/CD_4^+ Channels. The two points that are important to discuss here are whether CD_3^+ is formed by the hydride abstraction reaction (N1) or by the dissociative charge-transfer reaction (N1′) and how to explain the evolution of the CD_3^+/CD_4^+ ratio as a function of N^+ parent ion excitation. For this purpose, an energy diagram restricted to these channels is shown in Figure 9, which includes the levels associated with the excited ^2D and ^2P states of the neutral atom N and the first three excited states of NH.

It is clear from the work of Kunusoki and Ottinger,[30,31] who have observed the $NH(A^3\Pi \rightarrow X^3\Sigma^-)$ chemiluminescence in the $N^+(^3P) + CH_4$ reaction, that the H^- abstraction (channel N1), can account, at least in part, for the production of CH_3^+. They propose a two step mechanism, for collision energies from 1.6 up to 5 eV in the center of mass frame, compatible with their observations of the internal (rotational and vibrational) energy distributions of the $NH(A^3\Pi)$ product. The first step is the charge transfer from CH_4 to N^+, and in the second step, the resulting N atom takes away one H atom from the ionized methane to form $NH(A^3\Pi)$ in a stripping mechanism with no momentum transfer. This would lead to CH_3^+ products scattered in the backward hemisphere relative to the N^+ parent ion as observed in this work for the CD_3^+ product. The NH could also be formed in a lower state as for example in its ground-state $NH(X^3\Sigma^-)$. However, the mechanism proposed for the formation of the $NH(A^3\Pi)$ chemiluminescent state, might not be the same for the ground-state $NH(X^3\Sigma^-)$, whose formation is exothermic by more than 3 eV. Therefore, it is more difficult to predict where the CH_3^+ products associated with $NH(X^3\Sigma^-)$ would be scattered. Moreover, in this work, only relative cross sections are measured for the production of the $NH(A^3\Pi)$ chemiluminescent state;[30,31] therefore, we cannot estimate the total efficiency of the N1 channel only from these observations.

However, it is clear from our work that the charge transfer that also occurs as the production of CD_4^+, which is observed, can only be accounted for by the non dissociative charge transfer (N2); therefore, it is important to discuss whether the dissociative charge transfer (N1′) could also contribute to the CD_3^+ production.

The time-of-flight and axial velocity distributions shown in Figure 5 for CD_3^+ and CD_4^+ and the large value of their summed cross section suggest a near-resonant charge transfer. Moreover, this sum varies with collision energy as $(E_{CM})^{-0.23}$, which is a much less steep decrease than the Langevin cross section. A similar behavior, $(E_{CM})^{-1/3}$, is observed for the $Kr^+ + CH_4$ charge transfer, for which a resonant charge-transfer model reasonably accounts for this dependence.[66] Therefore, the observed data is very compatible with an efficient charge transfer.

We also looked to see if the CD_3^+/CD_4^+ ratio is compatible with such a mechanism. To discuss this point, it is very useful to compare it to the ratio of dissociated to undissociated products CD_3^+/CD_4^+ following the CD_4^+ fragmentation as a function of its internal energy. This information is known from the TPEPICO study of the dissociative photoionization of methane.[67] In this study, the energy for the crossover of the $CD_3^+ + D$ and the CD_4^+ curves in the CD_4^{+*} breakdown diagram[67] is at 14.3 eV above the CD_4 ground state. Above this energy, CD_4^+ rapidly dissociates into $CD_3^{+*} + D$. Because the recombination energy of N^+ is 14.53 eV, if we assume that all CD_3^+ ions come from the dissociative charge transfer, then the 0.82:0.18 ratio observed for the $N^+(^3P)$ reaction would correspond to an equivalent dissociation of CD_4^{+*} at 14.4 eV. This means that a near-resonant charge transfer between N^+ and CD_4 that is exothermic by only 0.1 eV is compatible with the observed ratio. At the other extreme, if we suppose that all CD_4^+ charge-transfer products remain undissociated, then it would correspond to a charge transfer that is exothermic by more than 0.3 eV. The comparison with the Kr^+ charge transfer with CH_4 is also useful for this discussion because the $N^+(^3P)$ recombination energy, 14.53 eV, is between the two recombination energies, 14.0 and 14.66 eV, of the Kr^+ spin−orbit states, $^2P_{3/2}$ and $^2P_{1/2}$, respectively. The $Kr^+ + CH_4$ reaction has been extensively studied for statistical mixtures of the spin−orbit states[66,68,69] or with selection of these states.[70,71] It was found that the charge transfer is near resonant and populates a range of CH_4^+ internal energies of ±0.5 eV around the Kr^+ recombination energy producing CH_3^+ and CH_4^+ ions essentially in the backward hemisphere. At thermal energies, the $Kr^+(^2P_{3/2})$ reaction leads to undissociated CH_4^+ products ,and the $Kr^+(^2P_{1/2})$ reaction leads to a 0.9:0.1 ratio of dissociated to undissociated products CH_3^+/CH_4^+. An intermediate ratio of 0.3:0.7 is found for a statistical population of the two Kr^+ spin−orbit states,[66] but it increases to 0.4:0.6 at 2 eV of collision energy. For the $Kr^+(^2P_{3/2})$ reaction, if the collision energy is large enough, then there is also a much more isotropic CH_3^+ production by an inelastic dissociative charge transfer in which translational energy is converted into internal energy.[69] This process is less efficient than the near-resonant charge transfer. At 1.2 eV, for instance, the CH_3^+ component represents about 15% of the $Kr^+(^2P_{3/2})$ reactivity, the remaining 85% being CH_4^+ products.[69] Our ratio of 0.82:0.18, which is quite constant with collision energy, is intermediate between the $Kr^+(^2P_{3/2})$ and $Kr^+(^2P_{1/2})$ values given above but closer from the latter, which is consistent with the intermediate value of the N^+ recombination energy, 14.53 eV. As a summary, the CD_3^+/CD_4^+ ratio is compatible with a near-resonant charge transfer and suggests that the dissociative charge transfer (N1′) could be the major channel to produce CD_3^+ ions.

The most striking effect of N^+ excitation in the ^1D state is the reversal of the CD_3^+ and CD_4^+ productions. If we assume that the CD_4^{+*} ions have already enough energy to fragment in the ground-state reaction, then it is surprising that when 1.9 eV is added by the N^+ excitation CD_4^{+*} ions are not completely dissociated. However, for both processes, (N1) and (N2), an analysis of the spin conservation rules should be made first.

For the H^- transfer, it is believed that the spin conservation rule is respected.[30,31] For the $N^+(^3P) + CD_4$ reaction, the

entrance channel is a triplet surface as is the observed exit channel, $ND(A^3\Pi) + CD_3^+$ and also the ground-state level, $ND(X^3\Sigma^-) + CD_3^+$. The N^+ excitation implies that the entrance channel is now a singlet surface, which cannot lead to the triplet surfaces $ND(X^3\Sigma^-, A^3\Pi) + CD_3^+$.[30,31] However, there are two ND singlet states, $a^1\Delta$ and $b^1\Sigma^-$, that lie between the X and A states (Figure 9), which could be populated according to the spin conservation rule in the $N^+(^1D) + CD_4$ reaction.

Whereas for the charge-transfer processes N2 and N1′, the situation is different. In the $N^+(^3P)$ recombination, doublet and quartet states of N are allowed to be formed, in particular, the lowest levels $N(^4S, ^2D, ^2P)$. However, in the $N^+(^1D)$ recombination, because only doublet states can be formed, the recombination toward the ground-state $N(^4S)$ is now forbidden and only the excited states $N(^2D, ^2P)$ are allowed to be formed. Thus, the two channels $CD_4^+ + N(^4S)$ and $CD_3^+ + D + N(^4S)$ are spin forbidden from the $N^+(^1D) + CD_4$ entrance channel, only the upper channels associated with $N(^2D)$ or $N(^2P)$ would be spin allowed. For the nondissociative charge transfer (N2), these $CD_4^+ + N(^2D)$ and $CD_4^+ + N(^2P)$ levels are energetically accessible from the $N^+(^1D) + CD_4$ entrance channel, but for the dissociative charge transfer (N1′), the $CD_3^+ + D + N(^2D)$ and $CD_3^+ + D + N(^2P)$ levels are not energetically accessible. Thus, the near-resonant nondissociative charge transfer (N2) is still possible, but the dissociative charge transfer (N1′) needs at least 0.3 eV collision energy to be converted into internal energy, which makes this process much less efficient, as reported for the $Kr^+ + CH_4$ reaction.[69] Thus, with N^+ excitation, the strong reduction of the N1′ channel seems to explain the observed decrease of CD_3^+ products and increase of the undissociated charge-transfer products, CD_4^+, well.

Moreover, if some of the remaining CD_3^+ products observed in the $N^+(^1D) + CD_4$ reaction would still come from the N1′ channel, then their velocity distribution would not be peaked in the backward hemisphere as observed but much more isotropically as that for the $Kr^+ + CH_4$ reaction;[69] therefore, it is most probable that this remaining fraction of CD_3^+ products comes from the D^- abstraction channel (N1) only. If the decrease of CD_3^+ products with N^+ excitation is interpreted as the closing of the N1′ channel, then it is reasonable to think that, for the ground-state $N^+(^3P)$ reaction, a comparable and small amount of CD_3^+ products is due to the N1 channel, which has no reason to be strongly affected by the N^+ excitation as discussed above.

To summarize, it seems that the near-resonant charge transfer, which can occur even at very large impact parameters, dominates. To explain the lower efficiency of the N1 channel, it could be possible that the D transfer occurs, following the charge transfer, only at smaller impact parameters. Apart from the competition between the N1, N2, and N1′ channels, N^+ excitation also reduces the overall efficiency of these processes compared to that of the N3 and N4 channels. It is possible that the competition between the formation of the complex and the charge and D transfer is more in favor of the former, which would explain the relative increase of DCN^+ and $DCND^+$ products with $N^+(^1D)$ excitation; for instance, the near-resonant part of the $Kr^+ + CH_4$ total (nondissociative and dissociative) charge transfer is known to be much less efficient for Kr^+ ($^2P_{1/2}$) than for Kr^+ ($^2P_{3/2}$),[69] although these two states are separated by only 0.66 eV.

B. $O^+ + CO_2$ Reaction. The principal results of this work, particularly the measurement of the cross sections for O_2^+ and CO_2^+ production for each of the two pure metastable states $O^+(^2D)$ and $O^+(^2P)$, which was done for the first time here, will be discussed in view of what was previously stated for this system,[37] at least for energies below a few eV, namely,

- the energy has a relatively small effect on the overall efficiency of the reaction

- any kind of energy has the same strong effect on enhancing the branching ratio into the charge-transfer channel (O2) leading to CO_2^+ at the expense of the O1 channel leading to O_2^+.

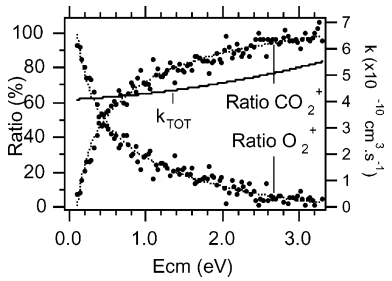

Figure 10. Branching ratio (dots and left scale) between O_2^+ and CO_2^+ products and total rate constant k_{TOT} (full line and right scale) for the $O^+(^4S) + CO_2$ reaction as a function of collision energy.

As observed in the literature for the ground-state reaction, we have seen a steep decrease in the O_2^+ product cross section with collision energy (Figure 6). It follows a $(E_{CM})^{-1.1}$ dependence, which has to be compared with the $(E)^{-0.8}$ and $(E_{CM})^{-1.2}$ dependence observed for O_2^+ production by Paulson et al.[48] and Flesh et al.[53], respectively, and to the $(v)^{-1.6}$ (i.e., $(E)^{-0.8}$) dependence observed by Johnsen et al.[50] (although it is not clear if it is for the O^+ disappearance cross section or for the O_2^+ production cross section). This deviation from the Langevin-capture cross-section dependence can be accounted for by the CO_2^+ production increase observed at the same time because the total cross section almost follows a Langevin dependence (the exponent is -0.47 instead of -0.5).

By multiplication by the mean relative velocity, the total cross section is converted into the total rate constant, shown in Figure 10. It varies slowly over a collision energy range of 3 eV, around a mean value of 5×10^{-10} cm^3 s^{-1}, which is slightly below the range of values, 6 to 12 $\times$ 10^{-10} cm^3 s^{-1}, found in the literature.[35,37−45,47−52]

In contrast, the branching ratio between the O_2^+ and CO_2^+ products varies rapidly with collision energy, as seen in Figure 10. CO_2^+ production is expected because the charge transfer endothermicity, 0.16 eV, can be, in part, overcome by collision energy or by internal energy, according to Viggiano.[37] If it is assumed that the reaction proceeds through a long-lived complex, as it is suggested by the product ion energy distribution for energies lower than 0.8 eV (ref 17 in ref 37), then the CO_2^+ ratio is surprisingly strong, in a statistical point of view that energetically favors the O_2^+ channel. A transition-state-theory-based modeling of this reaction[54] has incorporated a constant intersystem crossing rate constant of about 1×10^{11} s^{-1} for the transition from a quartet to a doublet CO_3^+ complex because this intersystem crossing is a prerequisite to the production of the low energy product $O_2^+ + CO$, which is a doublet. With the inclusion of this intersystem crossing rate constant of adequate magnitude, the model reasonably predicts the rate constant and the branching ratio for energies below 0.6 eV.[54]

In Figure 10, note that at larger collision energies, above 2 eV, the CO_2^+ branching ratio does not vary by more than 10% because it is already close to 100%, and the charge transfer cross section, which is close to the total cross section (Figure 6.) slowly decreases. It is not expected that, extrapolated to 5 eV collision energy, the efficiency of the charge transfer would be much higher. For the three state-selected $^4S/^2D/^2P$ reactions,

TABLE 2: Recombination Energies (eV) of Initial $O^+(^4S, ^2D, ^2P)$ States to Final Neutral $O(^3P, ^1D, ^1S)$ States and CO_2 Ionization Energies from Its Ground State to the Three CO_2^+ Excited States, $X^2\Pi_g$, $A^2\Pi_u$, and $B^2\Sigma_u^+$.

	initial O^+ state		
final O state	^4S	^2D	^2P
^3P	13.618	16.943	18.636
^1D	11.651	14.976	16.669
^1S	9.428	12.753	14.446
final CO_2^+ state	$X^2\Pi_g$	$A^2\Pi_u$	$B^2\Sigma_u^+$
E_i (eV)	13.776	17.310	18.065

whose excitation energy are 0:3.3:5 eV, the ratios of the cross sections, measured at 0.36 eV, are 1:0.85:1.40 for the total values and 1:1.61:2.63 for the charge transfer only. These values are not predictable by a model in which the electronic energy plays the same role as any kind of energy. In a statistical model, such as the one used for the ^4S reaction,[54] the reaction of O^+ in the doublet states ^2D or ^2P no longer requires an intersystem crossing to reach the doublet O_2^+ product channel. Thus, such a model would predict a higher fraction of O_2^+ products than it would for the ^4S reaction in complete contradiction with our measurements. We believe that the dynamics are different when the system starts from the excited surface $O^+(^2D, ^2P) + CO_2$.

It is reasonable to think that other parameters are driving the reaction and especially the charge transfer, such as energy defects and vibrational Franck Condon factors with all possible final states. All recombination energies of $O^+(^4S, ^2D, ^2P)$ states to neutral $O(^3P, ^1D, ^1S)$ states are compared in Table 2 with the ionization energies of CO_2 from its ground state to the first three excited states of CO_2^+, $X^2\Pi_g$, $A^2\Pi_u$, and $B^2\Sigma_u^+$.

The charge-transfer reaction from O^+ in the ^2D and ^2P excited states has quite different energy defects than those from the O^+ ground state ^4S; for instance, the ^2D recombination to the ^3P is not sufficient to reach the $A^2\Pi_u$ state (-0.37 eV), and its recombination to the ^1D is above the $X^2\Pi_g$ state ($+1.2$ eV). Whereas the ^2P recombination to the ^3P is just above the $B^2\Sigma_u^+$ state ($+0.57$ eV), and its recombination to the ^1S state is just above the $X^2\Pi_g$ state ($+0.67$ eV). By also considering the energy defects between CO_2 and CO_2^+ individual vibronic levels and their overlaps (Franck Condon factors), this could give an explanation of the much larger efficiency of the charge transfer relative to the complex formation products for the O^+ (^2D, ^2P) reaction.

Conclusions

We have shown that dissociative photoionization of N_2 and O_2 associated with threshold photoelectron−photoion coincidences (TPEPICO) is a good method to produce state-selected atomic ions, such as $N^+(^1D)$ and $O^+(^2D, ^2P)$, if a discrimination on atomic ions produced with recoil energy is applied. The main advantage of the method is its ability to produce pure reactant ions without broadening their translational energy, which is important for the study of reaction dynamics. This technique was applied for the first time to the study of the state-selected $^{15}N^+(^3P, ^1D) + CD_4$ and $O^+(^4S, ^2D, ^2P) + {}^{13}CO_2$ reactions.

For both reactions, there is a strong competition between the charge-transfer process and the formation of a long-lived complex. For the reaction of N^+ with methane, there is also an intermediate H^- abstraction process, which probably plays only a minor role.

Clearly, excitation of the parent atomic ion does not play the same role as other forms of energy because the charge transfer is very sensitive to the nature of the initial and final states and to small energy defects between them. A very clear example of this, for the reaction of N^+ with methane, is the very surprising reversal of dissociative to nondissociative charge transfer when the N^+ ion is excited from the ^3P ground state to the metastable ^1D state, even though this excitation brings 2 eV to the system. This is because, for the $N(^1D)^+ + CH_4$ reaction, among the exothermic channels, the two nondissociative charge-transfer channels $CH_4^+ + N(^2D)$ and $CH_4^+ + N(^2P)$ are spin allowed and that the dissociative charge-transfer channel $CH_3^+ + H + N(^4S)$ is spin forbidden. In this case, the spin conservation rule in the recombination step makes the reaction very sensitive to the initial state. For the O^+ reaction too, it is very surprising to see that the charge transfer so rapidly overcomes its endothermicity and becomes by far the major process. It has been suggested[54] that, within the complex, an intersystem crossing rate constant between the quartet surface of the $O^+ + CO_2$ reactants and the doublet surface of the $O_2^+ + CO$ products is necessary to understand the fast increase in the charge-transfer CO_2^+ product with energy. Our results for the charge-transfer $O^+(^2D)$ and $O^+(^2P)$ reactions with CO_2 show, however, that for this reaction also, the charge transfer is probably sensitive to energy defects and the nature of the states.

These reactions are also of great importance for the chemistry of Titan, Mars, and Venus' ionospheres, where long-lived metastable N^+ and O^+ ions can be formed and can react. For the reaction of $N^+(^3P, ^1D)$ with methane, at least for low collision energies, the excitation to ^1D state does not change the total rate constant much but strongly affects the branching ratio between products. For this reason, the state specific ^1D reactivity should be considered in models, as long as its population is large enough. For long-lived metastable $O^+(^2D, ^2P)$ ions, both the efficiency and the branching ratio between products are dependent on O^+ excitation. However, collision energy is also important to consider for models because a nonnegligible fraction of the N^+ or O^+ ions in these ionospheres can be formed with high translational energies from fast N_2^+ (O_2^+) or N_2^{2+} (O_2^{2+}) dissociation. Because the distributions of such translational energies extend beyond 5 eV, we have not yet explored the whole collision-energy range that would be necessary. For energies up to a few electronvolts, it is already clear that the branching ratios are very dependent on collision energy.

Acknowledgment. We thank the technical staff of LURE for operating the Super-ACO storage ring and are also grateful to the French "Programme National de Planétologie" lead by INSUE for funding this research activity. This paper is dedicated to Professor Tomas Baer, who has been a close collaborator of our group for many years and a dear friend of one of the authors.

References and Notes

(1) Baer, T.; Booze, J.; Weitzel, K.-M. Photoelectron-Photoion Coincidence Studies of Ion Dissociation Dynamics. In *Vacuum Ultraviolet Photoionization and Photodissociation of Molecules and Clusters*; Ng, C.-Y., Ed.; World Scientific Publishing Co. Pte. Ltd.: Singapore, 1991; p 259.

(2) Baer, T. State Selection by Photoion-Photoelectron Coincidence. In *Gas-Phase Ion Chemistry*; Bowers, M. T., Ed.; Academic Press: New York, 1991; Vol. 1; p 153.

(3) Ng, C. Y. Molecular beam photoionization and photoelectron-photoion coincidence studies of high-temperature molecules, transient species, and clusters. In *Vacuum Ultraviolet Photoionization and Photodissociation of Molecules and Clusters*; Ng, C.-Y., Ed.; World Scientific Publishing Co. Pte. Ltd.: Singapore, 1991; Vol. 169−257.

(4) Koyano, I.; Tanaka, K. State selected charge transfer and chemical reactions by the TESICO technique. In *State-Selected and State-to-State Ion−Molecule Reaction Dynamics. Part 1: Experiment*; Ng, C. Y., Baer, M., Eds.; John Wiley: New York, 1992; Vol. 82; p 263.

(5) Ng, C.-Y. State-selected and state-to-state ion−molecule reaction dynamics by photoionization and differential reactivity methods. In *State-Selected and State-to-State Ion−Molecule Reaction Dynamics. Part 1: Experiment*; Ng, C. Y., Baer, M., Eds.; John Wiley: New York, 1992; Vol. 82; p 401.

(6) Baer, T.; Guyon, P.-M. An historical introduction to threshold ionization. In *High-Resolution Laser Photoionization and Photoelectron Studies*; Powis, I., Baer, T., Ng, C., Eds.; John Wiley & Sons: Chichester, U.K., 1995; p 1.

(7) Ng, C. Y. *J. Phys. Chem. A* **2002**, *106*, 5953.

(8) Ng, C. Y. *Annu. Rev. Phys. Chem.* **2002**, *53*, 101.

(9) Wiese, W. L.; Fuhr, J. R.; Deters, T. M. *J. Phys. Chem. Ref. Data* **1996**, *25*, 1.

(10) Lavollee, M.; Henri, G. *J. Phys. B: At. Mol. Opt. Phys.* **1989**, *22*, 2019.

(11) Fox, J. L.; Sung, K. Y. *J. Geophys. Res.* **2001**, *106*, 21305.

(12) Banaszkiewicz, M.; Lara, L. M.; Rodrigo, R.; Lopez-Moreno, J. J.; Molina-Cuberos, G. J. *Icarus* **2000**, *147*, 386.

(13) Nagy, A. F.; Cravens, T. E. *Planet. Space Sci.* **1998**, *46*, 1149.

(14) Keller, C. N.; Anicich, V. G.; Cravens, T. E. *Planet. Space Sci.* **1998**, *46*, 1157.

(15) Dalgarno, A.; Fox, J. L. Ion chemistry in atmospheric and astrophysical plasmas. In *Unimolecular and Bimolecular Ion−Molecule Reaction Dynamics*; Ng, C. Y., Baer, T., Powis, I., Eds.; John Wiley & Sons: Chichester, U.K., 1994; p 1.

(16) Anicich, V. G. *J. Phys. Chem. Ref. Dat.* **1993**, *22*, 1469.

(17) Anicich, V. G.; McEwan, M. J. *Planet. Space Sci.* **1997**, *45*, 897.

(18) McEwan, M. J.; Scott, G. B. I.; Anicich, V. G. *Int. J. Mass Spectrom. Ion Proc.* **1998**, *172*, 209.

(19) Anicich, V. G.; Wilson, P.; McEwan, M. J. *J. Am. Soc. Mass Spectrom.* **2004**, *15*, 1148.

(20) Fox, J. L. *Rev. Geophys.* **1991**, *29*, 1110.

(21) Nicolas, C. Etudes de réactions ion-molécule de l'ionosphère de Titan: réactions de N_2^+ et N^+ avec différentes molécules d'hydrocarbures. Thèse en cotutelle, Université Paris XI, Orsay, France et Technische Universität, Chemnitz, Allemagne, 2002.

(22) Nicolas, C.; Alcaraz, C.; Thissen, R.; Zabka, J.; Dutuit, O. *Planet. Space Sci.* **2002**, *50*, 877.

(23) Witasse, O.; Dutuit, O.; Lilensten, J.; Thissen, R.; Zabka, J.; Alcaraz, C.; Blelly, P.-L.; Bougher, S. W.; Engel, S.; Andersen, L. H.; Seiersen, K. *Geophys. Res. Lett.* **2002**, *29*, 104.

(24) Witasse, O.; Dutuit, O.; Lilensten, J.; Thissen, R.; Zabka, J.; Alcaraz, C.; Blelly, P.-L.; Bougher, S. W.; Engel, S.; Andersen, L. H.; Seiersen, K. *Geophys. Res. Lett.* **2003**, *30*, 1360.

(25) Anicich, V. G.; Huntress, W. T., Jr.; Futrell, J. H. *Chem. Phys. Lett.* **1977**, *47*, 488.

(26) Smith, D.; Adams, N. G.; Miller, T. M. *J. Chem. Phys.* **1978**, *69*, 308.

(27) Tichy, M.; Raskshit, A. B.; Lister, D. G.; Twiddy, N. D.; Adams, N. G.; Smith, D. *Int. J. Mass. Spectrom. Ion Phys.* **1979**, *29*, 231.

(28) Dheandhanoo, N. G.; Johnsen, R.; Biondi, M. A. *Planet. Space Sci.* **1984**, *32*, 1301.

(29) Rowe, B. R.; Marquette, J. B.; Dupeyrat, G.; Fergusson, E. E. *Chem. Phys. Lett.* **1985**, *113*, 403.

(30) Kusunoki, I.; Ottinger, C. *J. Chem. Phys.* **1979**, *70*, 710.

(31) Kusunoki, I.; Ottinger, C. *J. Chem. Phys.* **1979**, *70*, 699.

(32) Lee, A. R.; Enos, C. S.; Brenton, A. G. *Chem. Phys.* **1991**, *150*, 275.

(33) Moran, T. F.; Wilcox, J. B. *J. Chem. Phys.* **1979**, *70*, 1467.

(34) Moran, T. F.; Wilcox, J. B. *J. Chem. Phys.* **1978**, *69*, 1397.

(35) Viggiano, A. A.; Morris, R. A.; Paulson, J. F. *J. Chem. Phys.* **1990**, *93*, 1483.

(36) Lindsay, B. G.; Sieglaff, D. R.; Smith, K. A.; Stebbing, R. F. *J. Phys. B: At. Mol. Opt. Phys.* **1999**, *32*, 4697.

(37) Viggiano, A. A.; Morris, R. A.; Vandoren, J. M.; Paulson, J. F. *J. Chem. Phys.* **1992**, *96*, 270.

(38) Fehsenfeld, F. C.; Ferguson, E. E.; Schmeltekopf, A. L. *J. Chem. Phys.* **1966**, *44*, 3022.

(39) Dunkin, D. B.; Fehsenfeld, F. C.; Schmeltekopf, A. L.; Ferguson, E. E. *J. Chem. Phys.* **1968**, *49*, 1365.

(40) Mosesman, M.; Huntress, W. T. J. *J. Chem. Phys.* **1970**, *53*, 462.

(41) Lindinger, W.; Fehsenfeld, F. C.; Schmeltekopf, A. L.; Ferguson, E. E. *J. Geophys. Res.* **1974**, *79*, 4753.

(42) Jaffe, S.; Klein, F. S. *Int. J. Mass Spectrom. Ion Phys.* **1974**, *14*, 459.

(43) Adams, N. G.; Smith, D. *Int. J. Mass Spectrom. Ion Phys.* **1976**, *21*, 349.

(44) Viggiano, A. A.; Morris, R. A.; Dale, F.; Paulson, J. F. *J. Chem. Phys.* **1990**, *93*, 1681.

(45) Smith, D.; Spanel, P.; Mayhew, C. A. *Int. J. Mass Spectrom. Ion Proc.* **1992**, *117*, 457.

(46) Walter, C. W.; Cosby, P. C.; Peterson, J. R. *J. Chem. Phys.* **1993**, *98*, 2860.

(47) Paulson, J. F.; Mosher, R. L. *Bull. Am. Phys. Soc.* **1962**, *7*, 633.

(48) Paulson, J. F.; Mosher, R. L.; Dale, F. *J. Chem. Phys.* **1966**, *44*, 3025.

(49) Schildcrout, S. M.; Franklin, J. L. *J. Chem. Phys.* **1969**, *51*, 4055.

(50) Johnsen, R.; Brown, H. L.; Biondi, M. A. *J. Chem. Phys.* **1970**, *52*, 5080.

(51) Rutherford, J. A.; Vroom, D. A. *J. Chem. Phys.* **1976**, *64*, 3057.

(52) Hunton, D. E.; Viggiano, A. A.; Morris, R. A.; Paulson, J. F.; Smith, D.; Adams, N. G. *J. Geophys. Res.* **1991**, *96*, 13881.

(53) Flesch, G. D.; Ng, C. Y. *J. Geophys. Res.* **1991**, *96*, 21403.

(54) Sawilowsky, E. F.; Klippenstein, S. J. *J. Phys. Chem. A* **1998**, *102*, 9811.

(55) Métayer-Zeitoun, C.; Alcaraz, C.; Anderson, S. L.; Palm, H.; Dutuit, O. *J. Phys. Chem. A* **1995**, *99*, 15523.

(56) Dutuit, O.; Alcaraz, C.; Gerlich, D.; Guyon, P. M.; Hepburn, J. W.; Métayer-Zeitoun, C.; Ozenne, J. B.; Schweizer, M.; Weng, T. *Chem. Phys.* **1996**, *209*, 177.

(57) Nicolas, C.; Alcaraz, C.; Thissen, R.; Vervloet, M.; Dutuit, O. *J. Phys. B: At. Mol. Opt. Phys.* **2003**, *36*, 2239−2251.

(58) Lafosse, A.; Brenot, J. C.; Golovin, A. V.; Guyon, P. M.; Hoejrup, K.; Houver, J. C.; Lebech, M.; Dowek, D. *J. Chem. Phys.* **2001**, *114*, 6605.

(59) Lafosse, A.; Brenot, J. C.; Guyon, P. M.; Houver, J. C.; Golovin, A. V.; Lebech, M.; Dowek, D.; Lin, P.; Lucchese, R. R. *J. Chem. Phys.* **2002**, *117*, 8368.

(60) Guyon, P. M.; Baer, T.; Ferreira, L. F. A.; Nenner, I.; Tabché-Fouhaillé, A.; Botter, R.; Govers, T. *J. Phys. B: At. Mol. Opt. Phys.* **1978**, *11*, L141.

(61) Richard-Viard, M.; Dutuit, O.; Lavollée, M.; Govers, T.; Guyon, P. M.; Durup, J. *J. Chem. Phys.* **1985**, *82*, 4054.

(62) Li, X.; Huang, Y. L.; Flesch, G. D.; Ng, C. Y. *Rev. Sci. Instrum.* **1995**, *66*, 2871.

(63) Li, X.; Huang, Y. L.; Flesch, G. D.; Ng, C. Y. *Rev. Sci. Instrum.* **1994**, *65*, 3724.

(64) Fisk, G. A.; McDonald, J. D.; Herschbach, D. R. *Discuss. Faraday Soc.* **1967**, *44*, 228.

(65) Talbi, D. *Chem. Phys. Lett.* **1999**, *312*, 291.

(66) Tosi, P.; Delvai, C.; Bassi, D.; Dmitriev, O.; Cappelletti, D.; Vecchiocattivi, F. *Chem. Phys.* **1996**, *209*, 227.

(67) Stockbauer, R. *J. Chem. Phys.* **1973**, *58*, 3800.

(68) Herman, Z.; Birkinshaw, K.; Pacak, V. *Int. J. Mass. Spectrom. Ion Processes* **1994**, *135*, 47.

(69) Herman, Z.; Friedrich, B. *J. Chem. Phys.* **1995**, *102*, 7017.

(70) Adams, N. G.; Smith, D.; Alge, E. *J. Phys. B: At. Mol. Opt. Phys.* **1980**, *13*, 3325.

(71) Giles, K.; Adams, N. G.; Smith, D. *J. Phys. B: At. Mol. Opt. Phys.* **1989**, *22*, 873.